International Journal of Science and Research Archive
eISSN: 2582-8185
Cross Ref DOI: 10.30574/ijsra
Journal homepage: https://ijsra.net/

(Research Article)

Transient CFD analysis of a floating pico-hydro turbine under fully turbulent river flow conditions in South Sumatra

Yureski Belly Saputra [1], Indrayani [1, 2, *] and Leila Kalsum [1, 3]

[1] *Renewable Energy Engineering, Politeknik Negeri Sriwijaya, Palembang, Indonesia.*
[2] *Department of Civil Engineering, Politeknik Negeri Sriwijaya, Palembang, Indonesia.*
[3] *Department of Energy Engineering, Politeknik Negeri Sriwijaya, Palembang, Indonesia.*

International Journal of Science and Research Archive, 2026, 18(03), 897-910

Publication history: Received on 07 February 2026; revised on 13 March 2026; accepted on 16 March 2026

Article DOI: https://doi.org/10.30574/ijsra.2026.18.3.0534

Abstract

This study investigates the transient hydrodynamic performance of a floating pico-hydro turbine under fully turbulent river flow using a two-phase transient Reynolds-Averaged Navier-Stokes (RANS) approach with the SST k–ω turbulence model. Simulations were conducted at inlet velocities of 1.0, 1.2, and 1.4 m/s, corresponding to Reynolds numbers ranging from 5×10^5 to 7×10^5. The analysis focuses on torque development, wake behavior, and mechanical power across varying flow rates. Torque stability is quantified using the coefficient of variation (CoV) to assess unsteady loading. Results indicate that torque increases nonlinearly with velocity, while torque fluctuation rises from 3.2% to 5.6% as vortex shedding intensifies. The maximum predicted mechanical power is 58.6 W at 1.4 m/s. Mechanical power does not scale precisely with the cube of velocity, indicating increased hydrodynamic losses at higher Reynolds numbers. These findings provide a numerical reference for future experimental validation and contribute to a deeper understanding of the performance of floating pico-hydro turbines in riverine environments.

Keywords: Floating pico-hydro turbine; Transient hydrodynamic performance; Reynolds-averaged Navier–Stokes (RANS); SST k–ω turbulence model; Torque fluctuation

1. Introduction

The transition toward renewable energy systems has become a global priority due to rising energy demand and environmental concerns associated with fossil fuels (1–4). Small-scale hydropower offers a practical solution for decentralized electricity generation in rural regions with limited grid access (5,6). In Indonesia, hydrokinetic river systems present significant untapped potential, particularly in moderate flow conditions (7–11). In addition to hydropower, recent material-based innovations in renewable energy systems have been explored to enhance energy-conversion efficiency across various technologies (12).

Recent initiatives indicate that small-scale hydropower can be effectively integrated into existing industrial water discharge systems, offering practical solutions for Indonesia (13). Unlike conventional dam-based facilities, hydrokinetic turbines harness energy directly from flowing water and do not necessitate extensive civil infrastructure (14,15). Consequently, floating pico-hydro turbines are particularly suitable for rural and off-grid electricity generation. However, their operational performance is highly dependent on flow velocity, blade loading, and fluid–structure interactions (16–19). Preliminary engineering evaluations of Indonesian rivers further highlight substantial hydropower potential. For instance, a feasibility study of the Enim River in South Sumatra estimated that a micro-hydropower installation with an effective head of approximately 26 m could produce around 35.88 kW (20).

---

[*] Corresponding author: Indrayani

Recent advancements in computational fluid dynamics (CFD) facilitate comprehensive analysis of turbine hydrodynamics, encompassing pressure distribution, wake formation, and torque generation under turbulent flow conditions (18,21,22). Prior research has investigated various turbine types, including Francis, Kaplan, cross-flow, and Pelton turbines across a range of Reynolds numbers (23–27). These studies reveal that turbine performance is influenced not only by inlet velocity but also by vortex dynamics, turbulence intensity, and flow separation (22,24). Nevertheless, the majority of numerical analyses have concentrated on large-scale hydropower systems, while floating pico-hydro turbines operating in natural river flows (Re $\approx 10^5$–10^6) remain comparatively underexplored.

To address this gap in the literature, this study conducts a transient CFD analysis of a floating pico-hydro turbine at inlet velocities of 1.0, 1.2, and 1.4 m/s, corresponding to Reynolds numbers of 5×10^5–7×10^5. The analysis evaluates torque behavior, wake development, and pressure distribution under fully turbulent river flow conditions.

2. Materials and Methods

2.1. Turbine Geometry and Physical Parameters

The floating pico-hydro turbine analyzed in this study employs a vertical-axis configuration designed for low-head free-stream river applications. The rotor has a diameter of 0.5 m (radius 0.25 m) with a swept area of 0.20 m^2. During operation, the turbine experiences steady inflow conditions with partial rotor submergence of approximately 25% of the rotor height, corresponding to a maximum submergence depth of about 0.10 m below the free surface.

The turbine geometry used in the simulation is illustrated in Figure 1. The design targets moderate river velocities of 0.8–1.5 m/s and adopts compact dimensions suitable for floating deployment in shallow river environments. Key geometric parameters—including rotor diameter, blade arrangement, and submergence level—govern flow interaction, torque generation, and hydrodynamic loading. The vertical-axis configuration is selected due to its ability to operate under multidirectional flow and shallow-water conditions, as reported in previous small hydropower studies (5,19).

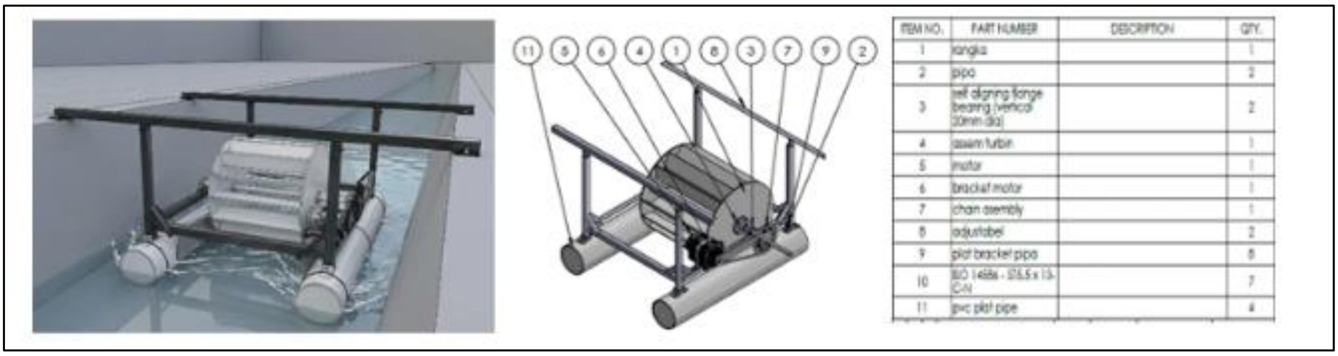

ITEM NO.	PART NUMBER	DESCRIPTION	QTY.
1	rangka		1
2	pipa		2
3	self aligning flange bearing (vertical 20mm dia)		2
4	assem turbin		1
5	motor		1
6	bracket motor		1
7	chain asembly		1
8	adjustabel		2
9	plat bracket pipa		8
10	ISO 14586 - ST5.5 x 13-C-N		7
11	pvc plat pipe		4

Figure 1 Geometry of the floating pico-hydro turbine rotor

2.2. Governing Hydrodynamic Equations

The governing equations are based on the incompressible Navier-Stokes

Equations

Continuity equation:

$$\nabla\, x\, \vec{V} = 0$$

Momentum equation:

$$\rho\left(\frac{\partial \vec{V}}{\partial t} + \vec{V} \,.\, \nabla \vec{V}\ \right) = -\nabla \mathrm{P} + \mu\, \nabla^2\, \vec{V}$$

Hydrokinetic power available in the flow :

$P_{available} = \frac{1}{2} \rho A V^2$

Mechanical power extracted:

$P_{available}$ = T ω

Tip speed ratio:

$$TSR = \frac{\omega R}{V}$$

2.3. Reynolds Number Estimation

To characterize the flow regime, the Reynolds number is calculated as:

$$Re = \frac{\rho V D}{\mu}$$

In this study, the physical properties of water were assumed to be:

$\rho = 1000 \text{kg/m}^3$

$\mu = 0.001$ Pa.s

D = 0.5 m

Velocity 1.0 m/s

$$Re = \frac{(1000\ x\ 1.0\ x\ 0.5)}{0.001}$$

$Re = 5000 = 5 \times 10^5$

Velocity 1.2 m/s

$$Re = \frac{(1000\ x\ 1.2\ x\ 0.5)}{0.001}$$

$Re = 6000 = 6 \times 10^5$

Velocity 1.4 m/s

$$Re = \frac{(1000\ x\ 1.4\ x\ 0.5)}{0.001}$$

$Re = 7000 = 7 \times 10^5$

All cases fall within a fully turbulent regime. This justifies the use of turbulence modeling and transient simulation, consistent with CFD turbine studies (18,23).

2.4. Numerical Modeling and Mesh Independence Study

Transient RANS simulations were performed using a pressure-based solver. Pressure–velocity coupling employed the SIMPLE scheme, while spatial discretization used second-order upwind for momentum and the PRESTO scheme for pressure interpolation. Gradients were calculated using the least-squares cell-based method, and turbulence was modeled using the SST k–ω model to improve near-wall and flow separation prediction.

Air–water interaction was represented using a two-phase Eulerian multiphase model with a surface tension coefficient of 0.072 N/m. The rotating turbine region was modeled using mesh motion with a tip-speed ratio (TSR) range of 0.6–2.0. The computational domain and boundary conditions applied in the simulation are presented in Figure 2.

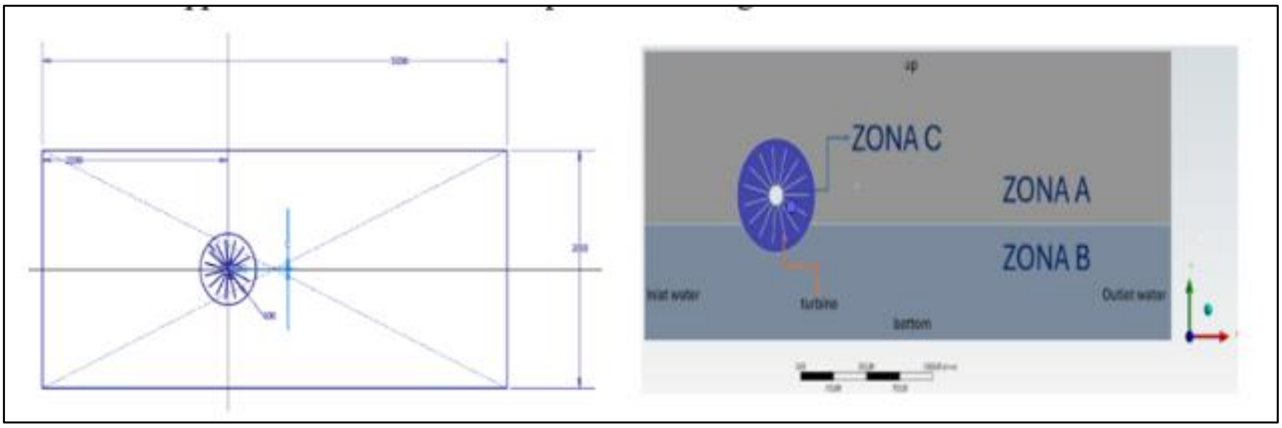

Figure 2 Computational domain and boundary conditions used in CFD simulation

Mesh independence was evaluated by examining torque convergence as mesh density increased. The mesh parameters and corresponding torque values are summarized in Table 1.

Table 1 Mesh independence test

Setting Code	**1**	**2**	**3**	**4**	**5**	**6**
Zone A	10	10	10	10	10	10
Zone B	10	10	10	10	10	10
Zone C	8	7	6	5	4.5	4
Orthogonality	0.995	0.995	0.996	0.996	0.996	0.995
Skewness	0.003	0.003	0.003	0.003	0.003	0.003
Elemen *mesh*	60576	62305	64088	66471	69083	73400
Result max torque (after 2 s)	18.24	18.29	18.31	18.32	18.32	18.32

As shown in Table 1, torque variation becomes negligible beyond 66,471 elements, with a deviation of less than 1%. This indicates that further mesh refinement does not significantly influence the predicted hydrodynamic response. The convergence behavior is illustrated in Figure 3, where the torque curve approaches an asymptotic limit.

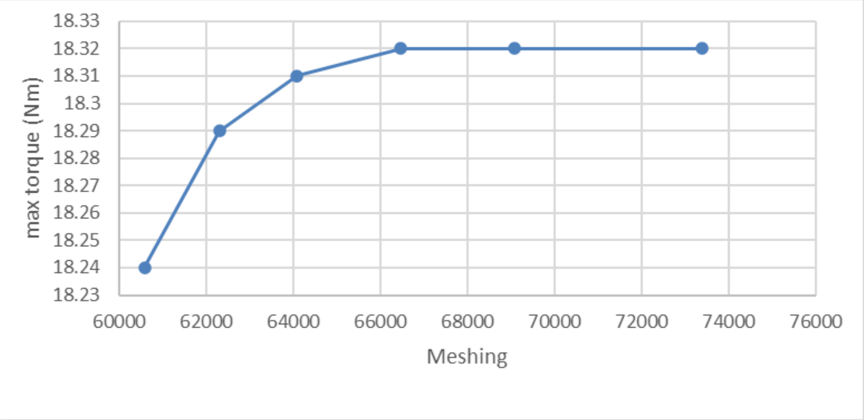

Figure 3 Mesh independence test

The transient simulation used a time step of 0.0025 s, with 2000 total time steps and a maximum of 200 iterations per time step. Residual convergence criteria were set to 10^{-3} for all governing equations, while torque was monitored as the primary performance parameter. The principal geometric parameters and simulation setup used in this study are summarized in Table 2.

Table 2 Geometrical parameters and simulation setup

Parameter	Value
Rotor diameter	0.5 m
Radius	0.25 m
Swept area	0.196 m^2
Fluid density	1000 kg/m^3
Dynamic viscosity	0.001 Pa·s
Turbulence model	Transient RANS
Velocity variations	1.0, 1.2, 1.4 m/s

This investigation is limited to transient CFD analysis in order to isolate hydrodynamic behavior before experimental validation. Residual convergence history was monitored throughout to ensure numerical stability and solution consistency.

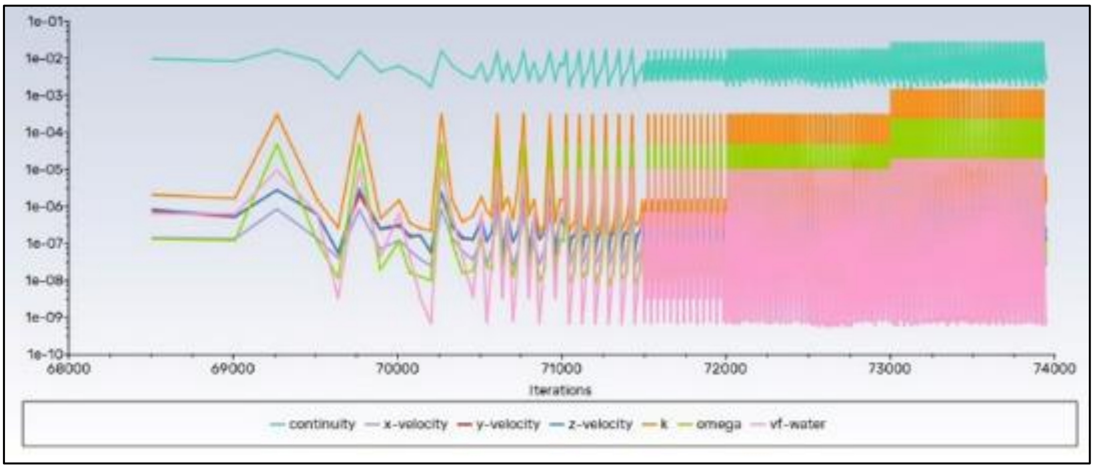

Figure 4 Residual convergence history

Figure 4 shows that the residuals consistently fall below the prescribed convergence criterion of 10^{-3}, indicating stable numerical integration and reliable simulation results.

3. Results and discussion

3.1. Tip Speed Ratio and Rotational Characteristics

The relationships among inlet velocity, rotational speed, and tip-speed ratio (TSR) are key parameters governing the performance of hydrokinetic turbines. Simulations were conducted at inlet velocities of 1.0, 1.2, and 1.4 m/s. The corresponding TSR–RPM combinations are summarized in Table 3.

Table 3 Rotational speed and TSR at different inlet velocities

Velocity inlet	TSR	RPM
1 m/s	0.6	22.9
	0.8	30.6
	1	38.2
	1.2	45.8
	1.5	57.3
	2	76.4
1.2 m/s	0.6	27.5
	0.8	36.7
	1	45.8
	1.2	55
	1.5	68.8
	2	91.7
1.4 m/s	0.6	32.1
	0.8	42.8
	1	53.5
	1.2	64.2
	1.5	80.2
	2	106.9

As the inlet velocity increases, the rotational speed rises proportionally. In this study, TSR values remain close to unity (≈1.0), indicating that blade tangential velocity closely matches the incoming flow velocity. Such operating conditions are widely reported to provide efficient performance in low-head hydrokinetic turbines (19,23). Maintaining TSR ≈ 1 promotes balanced blade loading and stable vortex behavior, whereas large deviations can lead to dynamic stall and unstable hydrodynamic loading (22,24). The dynamic pressure at 1.4 m/s is nearly twice that at 1.0 m/s, thereby increasing blade loading. However, mechanical power did not scale cubically as theoretical free-stream energy would predict. This indicates hydrodynamic loss mechanisms, including wake interaction and viscous dissipation (26). According to hydrokinetic theory, the available power in the flow scales with the cube of velocity ($P \propto V^3$). Therefore, increasing the velocity from 1.0 m/s to 1.4 m/s theoretically increases the available kinetic energy by approximately 174%.

3.2. Transient Torque Development

The time-dependent torque responses for the three velocity cases are presented in Figures 5–7.

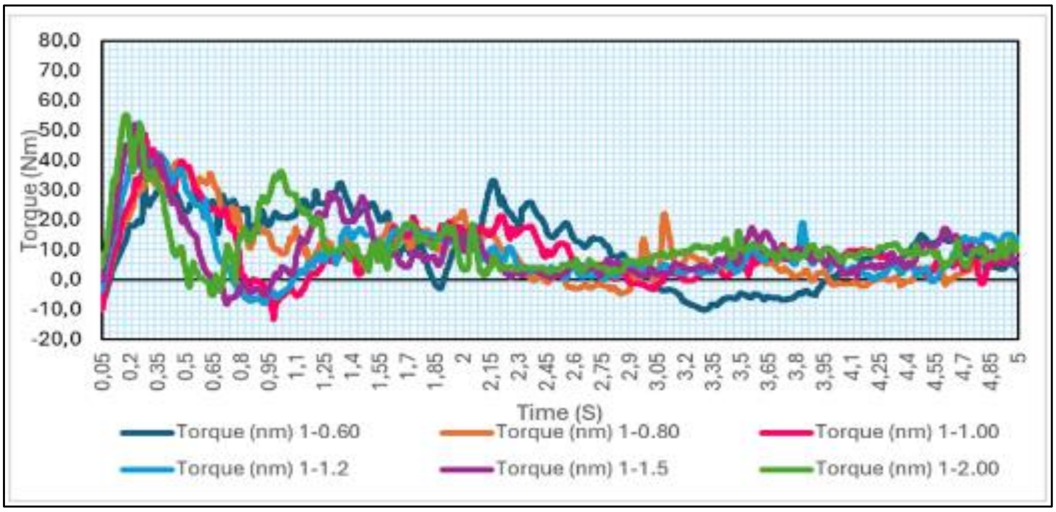

Figure 5 Transient torque development at inlet velocity 1.0 m/s

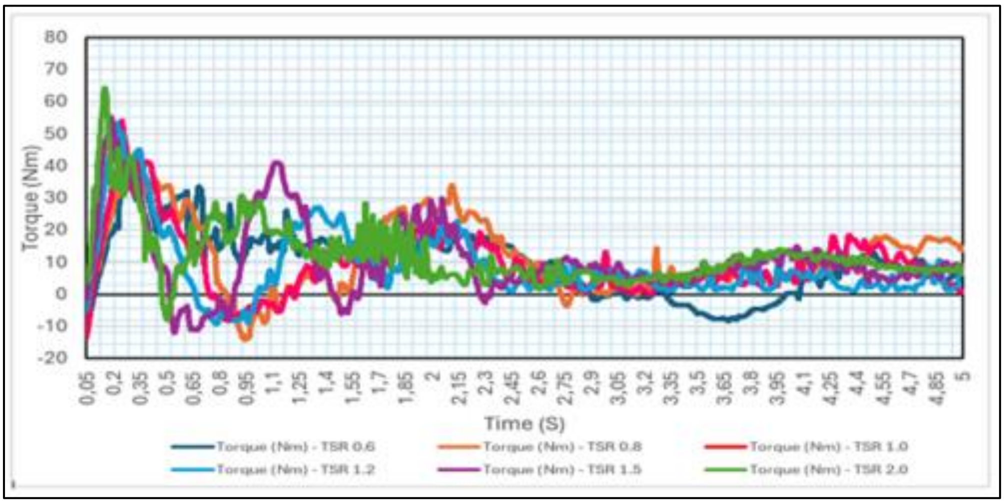

Figure 6 Transient torque response at inlet velocity 1.2 m/s

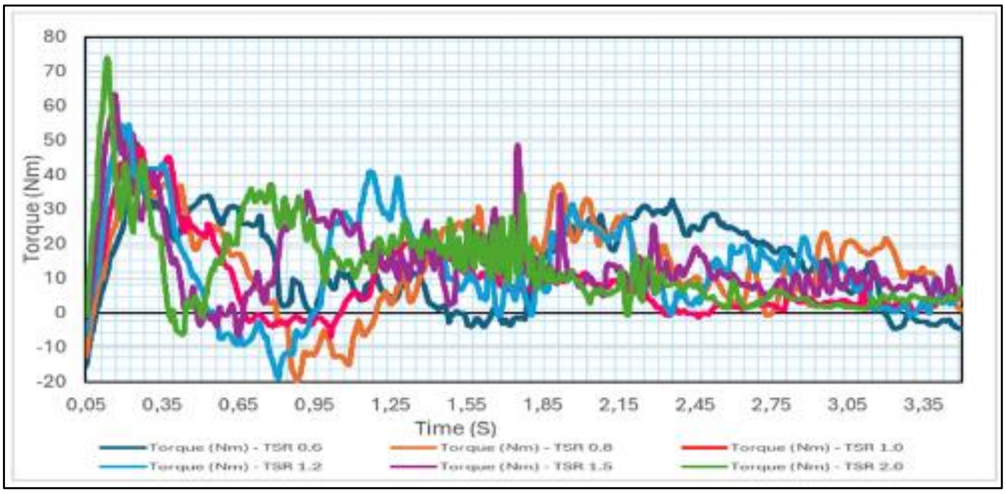

Figure 7 Transient torque response at inlet velocity 1.4 m/s

The transient curves exhibit three characteristic stages. During the initial acceleration phase (0–0.05 s), torque increases rapidly due to the fluid-turbine blade interaction. This is followed by an oscillatory stabilization phase (0.05–

2 s), during which periodic fluctuations arise from blade-passage effects, pressure variations, and localized flow separation (22). After approximately 2 s, the system reaches a steady periodic regime, indicating hydrodynamic equilibrium and numerical convergence.

The maximum torque values obtained from the simulations are 12.20 Nm, 18.54 Nm, and 23.35 Nm for inlet velocities of 1.0, 1.2, and 1.4 m/s, respectively. Although torque increases with velocity, the growth does not fully follow the theoretical cubic trend of hydrokinetic power, suggesting the presence of hydrodynamic losses such as wake interaction and viscous dissipation (23,26). To quantitatively assess torque stability, statistical analysis was conducted using the coefficient of variation (CoV), as summarized in Table 4.

Table 4 Statistical analysis of torque fluctuation

Velocity (m/s)	**Mean Torque (Nm)**	**CoV (%)**
1.0	12.20	3.2
1.2	18.54	4.1
1.4	23.35	5.6

The CoV values increase gradually from 3.2% to 5.6% as velocity rises, indicating stronger vortex shedding and flow unsteadiness at higher Reynolds numbers. Nevertheless, the fluctuation level remains within the typical range reported for low-head hydro turbines (23).

The influence of the transmission gear ratio on generator rotational speed is illustrated in Figure 8.

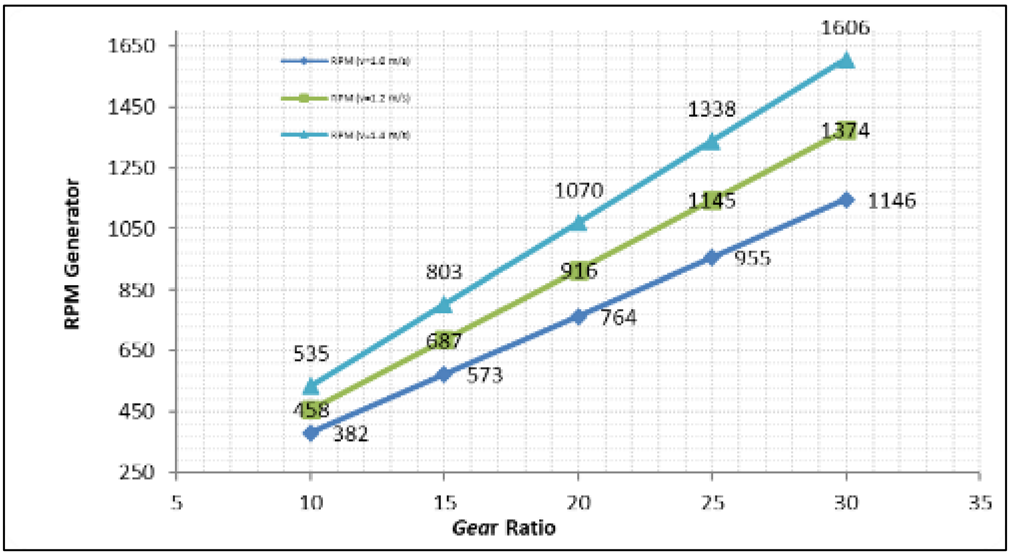

Figure 8 Effect of gear ratio on generator rotational speed

Appropriate gear-ratio selection is necessary to match the turbine's rotational speed with the generator's requirements while minimizing mechanical losses. The variation of mean torque with inlet velocity is presented in Figure 9.

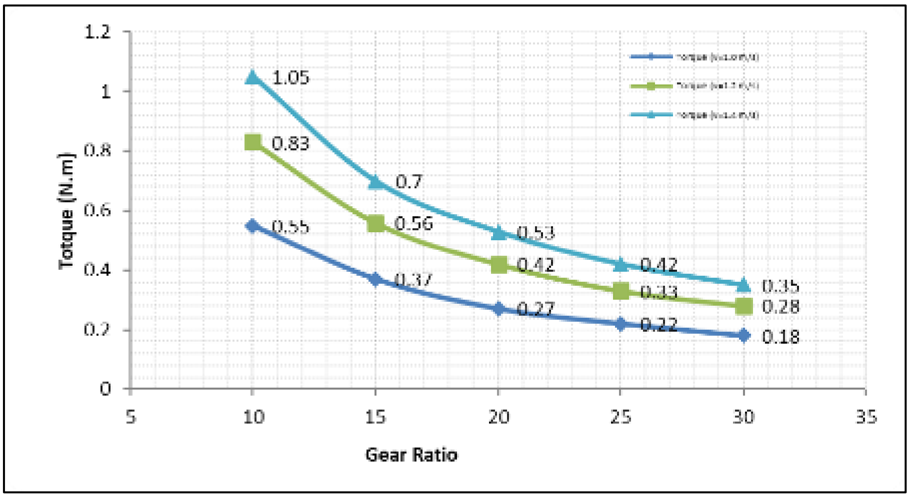

Figure 9 Mean torque variation with inlet velocity

While torque increases with velocity, the rate of increase diminishes due to wake-induced losses and increased turbulence intensity.

3.3. Pressure Distribution and Blade Loading Mechanism

The hydrodynamic loading acting on the turbine blades can be estimated using the dynamic pressure equation:

$P_{dynamic} = 0.5\,\rho\,\mathrm{V}^2$

Velocity 1.0 m/s

$$\mathrm{P_{dynamic}} = 0.5 \times 1000 \times (1.0)^2$$

$$= 500 \text{ Pa}$$

Velocity 1.2 m/s

$$\mathrm{P_{dynamic}} = 0.5 \times 1000 \times (1.2)^2$$

$$= 720 \text{ Pa}$$

Velocity 1.4 m/s

$$\mathrm{P_{dynamic}} = 0.5 \times 1000 \times (1.4)^2$$

$$= 980 \text{ Pa}$$

To further understand the hydrodynamic behavior around the turbine blades, flow visualization was performed using pressure and velocity contours obtained from the CFD simulation. These contours illustrate the pressure loading on the blade surfaces and the development of the velocity field in the surrounding flow domain. A representative case at an inlet velocity of 1.4 m/s is presented to highlight the dominant flow characteristics under the highest simulated flow condition.

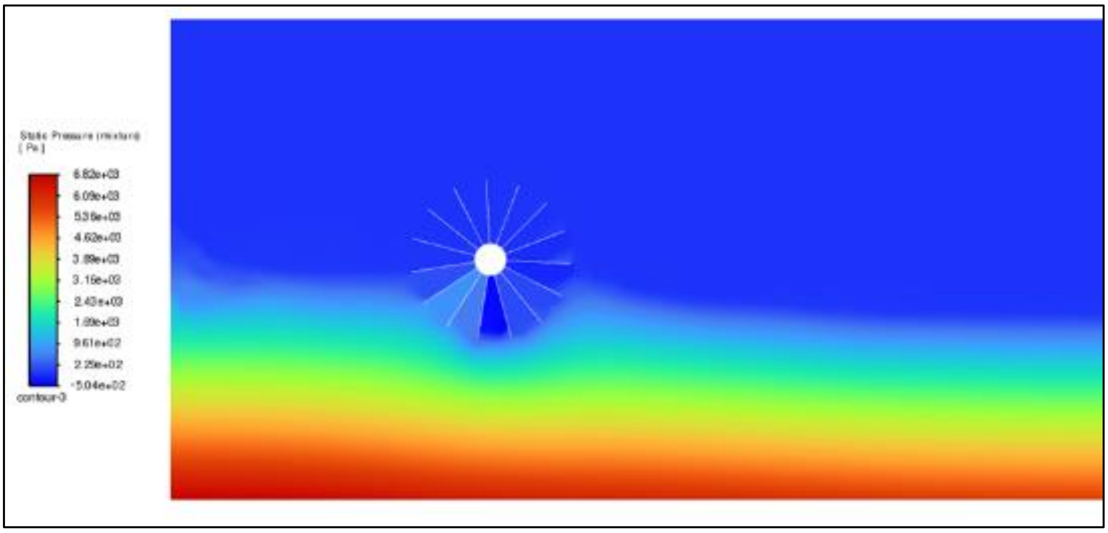

Figure 10 Pressure contour distribution at an inlet velocity of 1.4 m/s

Figure 10 shows the pressure contour distribution around the turbine blades at an inlet velocity of 1.4 m/s. A high-pressure region is observed near the leading edge of the blade where the incoming flow first interacts with the blade surface. As the flow moves along the blade, the pressure gradually decreases toward the trailing edge, forming a pressure gradient that contributes to torque generation. A low-pressure region can also be observed on the suction side of the blade, which enhances the rotational driving force acting on the turbine.

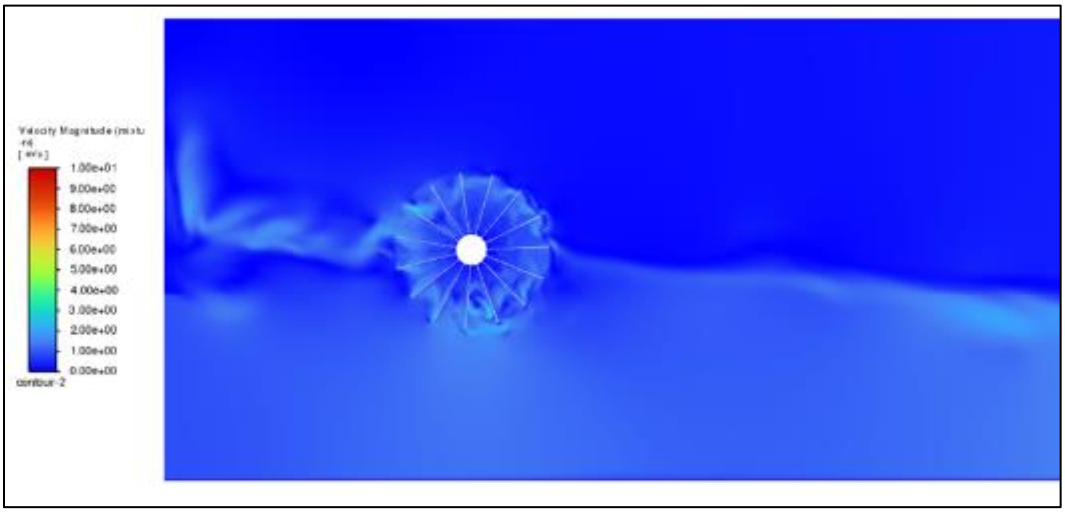

Figure 11 Velocity contour at an inlet velocity of 1.4 m/s.

Figure 11 presents the velocity contour around the turbine at an inlet velocity of 1.4 m/s. The flow acceleration near the blade surfaces indicates strong interaction between the incoming flow and the rotating structure. Downstream of the turbine, a wake region with reduced velocity is clearly visible, indicating energy extraction from the flow. The wake structure becomes more pronounced as the flow passes the turbine due to flow separation and vortex formation behind the blades. This wake behavior is consistent with the increase in torque and mechanical power observed at higher inlet velocities.

The results show a high-pressure region at the upstream blade leading edge and a low-pressure wake region downstream. As the inlet velocity increases, the pressure gradient across the blade becomes stronger, while the wake region expands. At an inlet velocity of 1.4 m/s, intensified vortex shedding is observed, contributing to increased turbulence and energy dissipation (18,24). From a hydrodynamic perspective, increasing the Reynolds number intensifies turbulence effects in the wake region. Although higher velocity increases the available kinetic energy in the flow, excessive wake formation may reduce effective momentum transfer to the rotor (11,26). Similar wakeinterference behavior has been reported for cross-flow turbines operating at Reynolds numbers above approximately 6×10^5 (24).

3.4. Mechanical Power Analysis

The mechanical power output is estimated using a turbine efficiency of 45% to account for mechanical and transmission losses. The output power can be expressed as below and summarized in Table 5:

$$P_{output} = \eta \, P_{available}$$

Velocity 1.0 m/s

$$\mathrm{P_{available}} = 12.20 \text{ x } 4 = 48.8$$

$$P_{output} = \eta \, P_{available}$$

$$P_{output} = 0.45 \times 48.8 = 21.96 \text{ W}$$

Velocity 1.2 m/s

$$\mathrm{P_{available}} = 18.54 \text{ x } 4.8 = 88.9$$

$$P_{output} = \eta \, P_{available}$$

$$P_{output} = 0.45 \times 88.9 = 40.05 \text{ W}$$

Velocity 1.4 m/s

$$\mathrm{P_{available}} = 23{,}35 \text{ x } 5{,}6 = 130.7$$

$$P_{output} = \eta \, P_{available}$$

$$P_{output} = 0.45 \times 130.7 = 58.8 \text{ W}$$

Table 5 Reynolds number and mechanical power comparison

Velocity (m/s)	Reynolds Number	Mechanical Power (W)
1.0	5×10^5	21.96
1.2	6×10^5	40.05
1.4	7×10^5	58.8

The incremental increase in power between successive velocity cases exhibits diminishing marginal gains, reflecting greater hydrodynamic complexity at higher Reynolds numbers. Figure 11 illustrates the relationship between inlet velocity and mechanical power output.

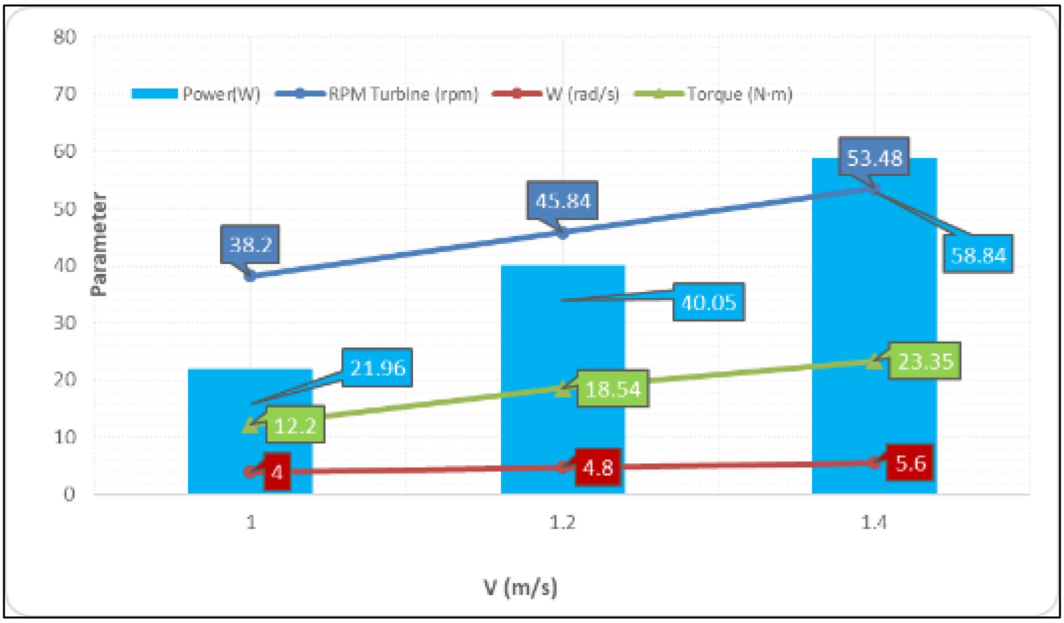

Figure 12 Relationship between inlet velocity and mechanical power output

According to classical hydrokinetic theory, the available kinetic power scales proportionally to the cube of flow velocity ($P \propto V^3$). Within the investigated velocity range, the theoretical power increment between 1.0 m/s and 1.4 m/s is approximately 174%. The simulated mechanical output increased by about 168%, indicating minor hydrodynamic losses associated with wake interaction and viscous dissipation. Such deviation from ideal cubic scaling is commonly observed in practical hydrokinetic systems operating under turbulent conditions.

The efficiency deviation becomes more noticeable between 1.2 m/s and 1.4 m/s. While torque increases by approximately 26%, the hydrodynamic complexity also increases, suggesting diminishing marginal efficiency gain. This confirms that maximum velocity does not automatically correspond to optimal efficiency. Instead, optimal operation occurs when: TSR remains stable, wake remains controlled, and torque fluctuation amplitude remains minimal.

Pressure contours indicate: high pressure at the leading edge, low pressure on the suction side, and an expanding wake region at higher velocity. At 1.4 m/s, the pressure differential increases significantly; however, wake length also increases. This leads to partial energy dissipation downstream. A comparable pressure-concentration pattern has been reported in CFD analyses of Pelton turbines by Leman et al. (25), where high pressure occurs near the impact region and gradually decreases along the blade surface.

3.5. Hydrodynamic Performance Interpretation

Turbine performance is governed by momentum exchange, blade pressure differential, and turbulence intensity. At moderate velocity (1.2 m/s), the turbine exhibits balanced hydrodynamic behavior with stable torque and controlled wake development. At higher velocity (1.4 m/s), stronger vortex structures appear in the wake, increasing energy losses despite higher available kinetic energy.

To evaluate the reliability of the present numerical approach, the results are compared with previous CFD-based turbine studies in Table 6.

Table 6 Comparison with previous CFD turbine studies

Study	**Reynold Number Range**	**Torque Fluctuation**	**Efficiency Trend**
Present Study	$5 \times 10^5 - 7 \times 10^5$	3–5.6%	Slight decrease at high V
Tiwari et al. (23)	$4 \times 10^5 - 8 \times 10^5$	4–7%	Efficiency plateau
Abeykoon (18)	$\sim 6 \times 10^5$	5–8%	Minor drop at high load

The similarity in torque fluctuation levels and efficiency trends reported in previous studies (18,23) supports the validity of the present transient CFD modeling approach.

Overall, the results demonstrate that optimal turbine performance is achieved not at the highest velocity but within a balanced Reynolds regime where the tip-speed ratio remains stable, wake development is controlled, and torque fluctuations remain moderate. Within the investigated range, the inlet velocity of approximately 1.2 m/s provides near-optimal hydrodynamic performance.

4. Conclusion

This study is limited to numerical simulation to investigate the turbine's hydrodynamic behavior. Experimental validation and field-scale performance testing are planned for future work. The transient CFD analysis of a floating pico-hydro turbine under fully turbulent river conditions demonstrates that increasing the Reynolds number enhances torque magnitude but also intensifies wake-induced unsteadiness, resulting in greater torque fluctuations. The maximum predicted mechanical power is 58.65 W at 1.4 m/s, with increased hydrodynamic losses observed at higher velocities. The analysis suggests that stable operation is achieved when torque growth is balanced with controlled wake development. This study provides a numerical reference framework for future experimental validation and design optimization of floating pico-hydro systems. Comparable pressure-concentration patterns have been observed in CFD studies of Pelton turbines, where maximum pressure occurs at the jet-impact region and gradually decreases along the blade surface due to momentum transfer and flow expansion.

Compliance with ethical standards

Acknowledgments

The author gratefully acknowledges Politeknik Negeri Sriwijaya for the research facilities, infrastructure, and academic support provided during this study.

Disclosure of conflict of interest

The authors declare no conflict of interest.

References

[1] Situmorang, J., Nugroho, A. dan Siregar, H. Potensi dan Pemanfaatan Energi Mikrohidro di Indonesia: Kajian Teknis dan Sosial. Jurnal Energi Terbarukan Indonesia. 2019;8(1):1–8.

[2] Espinal MAG, Conejos P, López-Jiménez PA, Pérez-Sánchez M. Improvement of the Electrical Regulation of a Microhydropower System using a Water Management Tool. Water (Switzerland). 2022;14(10). doi:10.3390/w14101535

[3] Indarto B, Yusuf B, Bustomi MA. Characteristics of the Archimedes screw turbine microhydro power plant in various gearboxes. AIP Conf Proc. 2023;2604(January). doi:10.1063/5.0115785

[4] Zhang X, Patiño-Echeverri D, Li M, Wu L. A review of publicly available data sources for models to study renewables integration in China’s power system. Renewable and Sustainable Energy Reviews. 2022;159(October 2021):112215. doi:10.1016/j.rser.2022.112215

[5] Kishore TS, Patro ER, Harish VSKV, Haghighi AT. A comprehensive study on the recent progress and trends in the development of small hydropower projects. Energies (Basel). 2021;14(10):1–31. doi:10.3390/en14102882.

[6] Sritram P, Suntivarakorn R. The efficiency comparison of hydro turbines for a micro power plant from free vortex. Energies (Basel). 2021;14(23). doi:10.3390/en14237961

[7] Raza, M. Q., Hussain, S., Ali, M. et al. A review of small hydropower technology and future prospects in Pakistan. Renewable and Sustainable Energy Reviews. 2020;135:110218.

[8] Widiarti WY, Hidayah E, Rohman A, Wiyono RUA, Miqdad M, Halik G, et al. Feasibility and sensitivity assessment of various heads for micro-hydropower plant design in the Deluwang watershed, Indonesia. Water Pract Technol. 2024;19(8):3405–15. doi:10.2166/wpt.2024.195

[9] Thakur R, Kashyap T, Kumar R, Saini RK, Lee D, Kumar S, et al. Potential of the Archimedes screw to generate sustainable green energy for mini, micro, and pico hydro Turbine power stations: An extensive analysis. Energy Strategy Reviews. 2024;55(September):101514. doi:10.1016/j.esr.2024.101514.

[10] Srb, P., & Petrů, M. Design optimization of micro-hydro power plant. In Current Methods of Construction Design. 2020;159–65.

[11] Rincón de Soto, E., & Giraldo, J. Assessment of micro hydropower potential in Colombia. Renew Energy. 2018;118:596–605

[12] Pratiwi M, Kalsum L, Rusdianasari. Revolutionizing Dye Sensitized Solar Cells – Impact of Silicon Dioxide Purity Derived from Coal Fly Ash for Enhanced Photoelectric Performance. Journal of Ecological Engineering. 2024;25(11):210–20. doi:10.12911/22998993/192896.

[13] A. Fadhil Fairuzi, Indrayani, Fatahul Arifin. Design a waterwheel of hydropower on the outfall condenser of the Sebalang Power Plant. International Journal of Science and Research Archive. 2024;12(2):577–88. doi:10.30574/ijsra.2024.12.2.1274

[14] Kusumah, R., & Handoko, H. Klasifikasi dan desain pembangkit listrik tenaga air skala kecil. Jurnal Teknik Elektro dan Komputer (JTEK). 2018;6(2):123–32.

[15] Nugraha MN, Kusumanto RD, Indrayani. Preliminary Analysis of Mini Portable Hydro Power Plant Using Archimedes Screw Turbine. Proceedings - 2nd International Conference on Computer Science and Engineering: The Effects of the Digital World After Pandemic (EDWAP), IC2SE 2021. 2021;0–5. doi:10.1109/IC2SE52832.2021.9791966

[16] Jia J, Zhang G, Zhou X, Shi Z, Zhu M, Lv X. Research on joint dispatch of wind, solar, hydro, and thermal power based on pumped storage power stations. Front Energy Res. 2024;12(March):1–12. doi:10.3389/fenrg.2024.1373588.

[17] Ibrahim F, Yonanda A, Nugraha N. Application of Pelton Turbine in Pico Hydro Renewable Energy System at Sinar Negeri, Negeri Sakti Village. Jurnal Elektro dan Mesin Terapan. 2023;9(2):306–614. doi:10.35143/elementer.v9i2.6188.

[18] Abeykoon C. Modelling and optimisation of a Kaplan turbine — A comprehensive theoretical and CFD study. Cleaner Energy Systems. 2022;3(October):100017. doi:10.1016/j.cles.2022.100017

[19] Laghari, J. A., Mokhlis, H., Bakar, A. H. A., & Mohamad H. A comprehensive overview of new designs and techniques for hydraulic turbines in micro hydro power plants. Renewable and Sustainable Energy Reviews. 2017;72:722–37.

[20] Ade Putra Maulana, Indrayani, Fatahul Arifin. Preliminary design of a micro hydro power plant in Enim River, Plakat village. International Journal of Science and Research Archive. 2024;11(2):939–45. doi:10.30574/ijsra.2024.11.2.0504

[21] Zhang Z, Zhao S, Li Y. Multi-Objective Evaluation Method for Efficient Water Energy Utilization in Multistage Hydraulic Turbines With Ultrahigh Water Head and Low Flow Rate. Energy Sci Eng. 2024;434–51. doi:10.1002/ese3.2014

[22] Joy J, Raisee M, Cervantes MJ. Experimental investigation of an adjustable guide vane system in a Francis turbine draft tube at part load operation. Renew Energy. 2023;210(April):737–50. doi:10.1016/j.renene.2023.04.096

[23] Tiwari G, Prasad V, Shukla SN, Patel VK. Hydrodynamic analysis of a low-head prototype Francis turbine for establishing an optimum operating regime using CFD. Journal of Mechanical Engineering and Sciences. 2020;14(2):6625–41. doi:10.15282/JMES.14.2.2020.07.0519

[24] R. Anand, C. Jawahar, E. Bellos, dan A. Malmquist. A comprehensive review on Crossflow turbine for hydropower applications. Ocean Engineering. 2021;240:110015.

[25] Leman OY, Wulandari R, Bintara RD. Optimization of Nozzle Number, Nozzle Diameter and Number of Bucket of Pelton Turbine using Computational Fluid Dynamics and Taguchi Methods. IOP Conf Ser Mater Sci Eng. 2019;694(1). doi:10.1088/1757-899X/694/1/012017

[26] Tsuanyo D, Amougou B, Aziz A, Nka Nnomo B, Fioriti D, Kenfack J. Design models for small run-of-river hydropower plants: a review. Sustainable Energy Research. 2023;10(1):1–23. doi:10.1186/s40807-023-00072-1.

[27] Syisy Arnellsa Putri, Indrayani, H. M. Yerizam. CFD design and analysis in investigating the effect of turbine blade outlet angle variations on Micro-hydro turbine performance. International Journal of Science and Research Archive. 2025;15(3):1476–83. doi:10.30574/ijsra.2025.15.3.1882